Appl. Math. Mech. -Engl. Ed. **30**(12), 1569–1578 (2009)
DOI: 10.1007/s10483-009-1208-6

Applied Mathematics and Mechanics (English Edition)

MHD flow of a viscous fluid on a nonlinear porous shrinking sheet with homotopy analysis method *

S. Nadeem, Anwar Hussain

(Department of Mathematics, Quaid-i-Azam University, 45320 Islamabad, Pakistan)

(Communicated by Zhe-wei ZHOU)

Abstract The present paper investigates the magnetohydrodynamic (MHD) flow of a viscous fluid towards a nonlinear porous shrinking sheet. The governing equations are simplified by similarity transformations. The reduced problem is then solved by the homotopy analysis method. The pertinent parameters appearing in the problem are discussed graphically and presented in tables. It is found that the shrinking solutions exist in the presence of MHD. It is also observed from the tables that the solutions for $f''(0)$ with different values of parameters are convergent.

Key words MHD flow, stagnation flow, shrinking sheet, homotopy analysis method

Chinese Library Classification O361.3
2000 Mathematics Subject Classification 76E25

Introduction

The phenomena of velocities on the boundary towards a fixed point are known as shrinking phenomena, which often occur in the situations such as rising shrinking balloon. Only limited attention has been focused on the study of shrinking phenomena[1-9]. However, in certain situations, the shrinking sheet solutions do not exist since the vorticity can not be confined in a boundary layer. These solutions may exist if either the magnetic field or the stagnation flow is taken into account. It is worth mentioning that the flow of an electrically conducting fluid past a porous plate under the effect of a magnetic field has attracted the attention of many investigators in view of its applications in many engineering problems such as magnetohydrodynamic (MHD) generators, plasma studies, nuclear reactors, oil exploration, geothermal energy extractions, and the boundary layer control in the field of aerodynamics. A number of MHD studies discuss the effects of magnetic fields on the hydrodynamic flow in various configurations[10-17].

The purpose of the present paper is to discuss the analytic solutions of the two-dimensional electrically conducting viscous fluid past a porous nonlinear porous shrinking sheet. To the best of the authors' knowledge, nonlinear shrinking sheet phenomena have not been considered by anyone. The governing equations are simplified by a suitable similarity transformation, and the reduced nonlinear boundary value problem is then solved analytically by the homotopy analysis method (HAM). Some recent works on the HAM have been published[18-28].

The physical behaviours of pertinent parameters on the velocity and skin friction are shown graphically and presented in tables. The convergence of the solution has been discussed through the $\hbar$-curves.

* Received Feb. 12, 2009 / Revised Aug. 25, 2009
Corresponding author S. Nadeem, E-mail: snqau@hotmail.com

1 Mathematical formulation

Consider the steady two-dimensional MHD flow of an incompressible viscous fluid over a nonlinear porous shrinking sheet at $y = 0$. The fluid is electrically conducting under the influence of an applied magnetic field $B(x)$ normal to the shrinking and porous sheet. The induced magnetic field is neglected. The governing equations for the flow problem are

$$\frac{\partial u}{\partial x} + \frac{\partial v}{\partial y} = 0, \tag{1}$$

$$u\frac{\partial u}{\partial x} + v\frac{\partial u}{\partial y} = \nu\frac{\partial^2 u}{\partial y^2} - \sigma\frac{B_0^2(x)}{\rho}u, \tag{2}$$

where u and v are the velocity components in the x and y directions, respectively, ν is the kinematic viscosity, ρ is the density, and σ is the electrical conductivity of the fluid. In Eq. (2), the external electric field and polarization effects are negligible[17]. Thus,

$$B(x) = B_0 x^{\frac{n-1}{2}}. \tag{3}$$

The boundary conditions corresponding to the nonlinear porous shrinking sheet are given as

$$u(x,0) = -cx^n,\ v(x,0) = -V_0 x^{\frac{n-1}{2}},\quad u(x,y) \to 0 \text{ as } y \to \infty, \tag{4}$$

where V_0 is the porousity of the plate. We introduce the similarity variables and non-dimensional variables as follows:

$$\eta = \sqrt{\frac{c(n+1)}{2\nu}}x^{\frac{n-1}{2}}y\ ,\ \ u = cx^n f^{'}(\eta), \tag{5}$$

$$v = -\sqrt{\frac{c\nu(n+1)}{2}}x^{\frac{n-1}{2}}[f(\eta) + \frac{n-1}{n+1}\eta f'(\eta)]. \tag{6}$$

Making use of Eqs. (5) and (6), the incompressibility condition is automatically satisfied. The momentum equations take the form

$$f''' + ff'' - \beta f^{'^2} - Mf' = 0. \tag{7}$$

The boundary conditions for the problem under consideration are

$$f(0) = K,\quad f'(0) = -1,\quad f'(\infty) = 0, \tag{8}$$

where K is the wall mass transfer parameter, M is the magnetic parameter, and β is the non-dimensional parameter. They are given as follows:

$$\beta = \frac{2n}{n+1},\quad M = \frac{2\sigma B_0^2}{\rho c(1+n)},\quad K = \frac{V_0}{\sqrt{\frac{c\nu(n+1)}{2}}}. \tag{9}$$

2 HAM solution

To seek the HAM solution to Eq. (7), we select

$$f(\eta) = K - 1 + \exp(-\eta) \tag{10}$$

as the initial approximation of f, and

$$\mathcal{L}\left[\widehat{f}(\eta;p)\right] = \frac{\partial^3\widehat{f}(\eta;p)}{\partial\eta^3} + \frac{\partial^2\widehat{f}(\eta;p)}{\partial\eta^2} \tag{11}$$

as the auxiliary linear operator that satisfies

$$\mathcal{L}\left[C_1 + C_2\mathrm{e}^{\eta} + C_3\mathrm{e}^{-\eta}\right] = 0, \tag{12}$$

where C_i $(i = 1,\ 2,\ 3)$ are arbitrary constants. If $p \in [0, 1]$ is an embedding parameter and $\hbar$ is a non-zero auxiliary parameter, the zeroth-order deformation problem is

$$(1-p)\,\mathcal{L}\left[\widehat{f}\,(\eta;p) - f\,(\eta)\right] = p\hbar\mathcal{N}\left[\widehat{f}\,(\eta;p)\right], \tag{13}$$

$$\widehat{f}\,(0;p) = K, \quad \widehat{f}\,'(0;p) = 1, \quad \widehat{f}\,'(\infty;p) = 0, \tag{14}$$

where

$$\mathcal{N}\left[\widehat{f}\,(\eta;p)\right] = \frac{\partial^3\widehat{f}\,(\eta;p)}{\partial\eta^3} + \widehat{f}\,(\eta;p)\,\frac{\partial^2\widehat{f}\,(\eta;p)}{\partial\eta^2} - \beta\left(\frac{\partial\widehat{f}\,(\eta;p)}{\partial\eta}\right)^2 - M^2\frac{\partial\widehat{f}\,(\eta;p)}{\partial\eta}, \tag{15}$$

and the mth-order deformation problem is

$$\mathcal{L}\left[f_m\,(\eta) - \chi_m f_{m-1}\,(\eta)\right] = \hbar\mathcal{R}_m\,(\eta)\,, \tag{16}$$

$$f_m\,(0) = 0, \quad f'_m\,(0) = 0, \quad f'_m\,(\infty) = 0, \tag{17}$$

$$\mathcal{R}_{1m}\,(\eta) = f'''_{m-1}\,(\eta) - M^2 f'_{m-1}\,(\eta) + \Sigma_{k=0}^{m-1}\left[f_{m-1-k}f''_k - \beta f'_{m-1-k}f'_k\right], \tag{18}$$

where

$$\chi_m = \begin{cases} 0, & m \le 1, \\ 1, & m > 1. \end{cases} \tag{19}$$

The symbolic software Mathematica is used to get the solution to Eq. (16) up to the first few orders of approximations. It is found that the solution for f is given by

$$f\,(\eta) = \sum_{m=0}^{\infty} f_m\,(\eta) = \lim_{N\to\infty}\left[\sum_{m=0}^{N} a^0_{m,0} + \sum_{n=1}^{2N+1}\mathrm{e}^{-n\eta}\left(\sum_{m=n-1}^{2N} a_{m,n}\right)\right], \tag{20}$$

in which the coefficient $a_{m,n}$ of $f_m\,(\eta)$ can be found by using given boundary conditions and with the initial guess approximation in Eq. (10). Also, the numerical data are presented graphically. $a_{m,n}$ is computed in Appendix.

3 Convergence of the analytic solution and discussions

The analytic series solutions of the considered problem presented in Eq. (20) have been found by the HAM. The expression contains the non-zero auxiliary parameter $\hbar$, which can adjust and control the convergence of the solutions. As pointed by Liao[21], to ensure the convergence of the solutions in the admissible range of the values for the auxiliary parameter $\hbar$, one can draw $\hbar$-curves.

In the present case, the 20th, 20th, and 17th orders of $\hbar$-curves are plotted in Figs. 1–3 for the non-dimensional magnetic parameter M, the non-dimensional mass suction parameter K, and the non-dimensional parameter β. It is seen from these figures that the admissible range for the values of $\hbar$ is $-1.7 \le \hbar \le -0.8$.

The results of different orders of approximations for the HAM solutions with M, K, and β are presented in Tables 1–3. It is observed from the tables that the values of $f''(0)$ increase with the increase of M, K, and β.

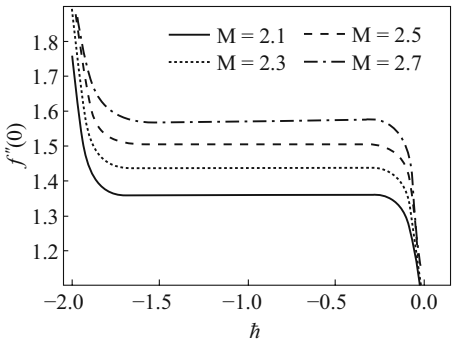

Fig. 1 The $\hbar$ curves for f for different M with $\beta = 0.1$ and $K = 0.1$

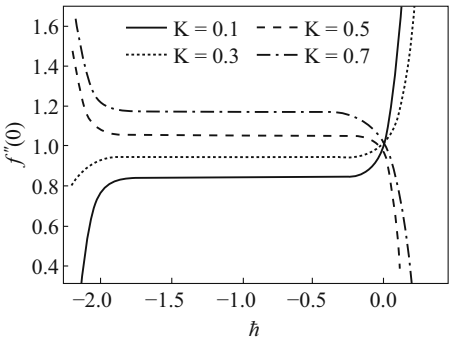

Fig. 2 The $\hbar$ curves for f for different K with $\beta = 0.1$ and $M = 1$

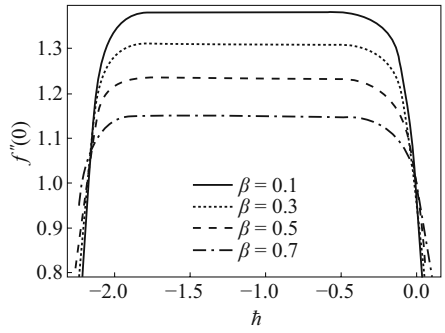

Fig. 3 The $\hbar$ curves for f for different β with $M = 1$ and $K = 1$

Table 1 Different orders of approximations of HAM solutions for M at $\hbar = -1$ with $\beta = 0.1$, $K = 1$

M	10th order	15th order	20th order	25th order	30th order	35th order	40th order
2.0	1.618 10	1.618 06	1.618 05	1.618 04	1.618 04	1.618 04	1.618 04
2.1	1.661 97	1.661 92	1.661 91	1.661 90	1.661 90	1.661 90	1.661 90
2.2	1.704 23	1.704 18	1.704 17	1.704 16	1.704 16	1.704 16	1.704 16
2.3	1.745 05	1.745 00	1.745 00	1.744 99	1.744 99	1.744 99	1.744 99
2.4	1.784 56	1.784 53	1.784 53	1.784 53	1.784 52	1.784 52	1.784 52
2.5	1.822 89	1.822 88	1.822 88	1.822 88	1.822 88	1.822 88	1.822 88
2.6	1.860 13	1.860 15	1.860 15	1.860 15	1.860 15	1.860 15	1.860 15
2.7	1.896 39	1.896 43	1.896 42	1.896 42	1.896 42	1.896 42	1.896 42
2.8	1.931 75	1.931 78	1.931 78	1.931 78	1.931 78	1.931 78	1.931 78
2.9	1.966 27	1.966 29	1.966 29	1.966 29	1.966 29	1.966 29	1.966 29
3.0	2.000 01	2.000 00	2.000 00	2.000 00	2.000 00	2.000 00	2.000 00

The effects of the mass suction parameter K, the magnetic parameter M, and the non-dimensional parameter β are shown in Figs. 4–7.

The velocity profiles for K at $M = 4$, $\beta = 1$ and $M = 1$, $\beta = 1$ are shown in Figs. 4 and 5, respectively. It is evident from Fig. 4 that when K increases, the velocity profiles are far away from the wall for mass injection, and the boundary layer thickness is more and more thicker. From Fig. 5, we can see that the boundary layer is near the wall for large K. Therefore, it is

Table 2 Different orders of approximations of HAM solutions for K at $\hbar = -1$ with $M = 2$, $\beta = 0.1$

K	10th order	15th order	20th order	25th order	30th order	35th order	40th order
0.0	1.270 98	1.270 95	1.270 95	1.270 95	1.270 95	1.270 94	1.270 94
0.1	1.318 80	1.318 75	1.318 74	1.318 74	1.318 74	1.318 74	1.318 74
0.2	1.368 64	1.368 58	1.368 56	1.368 56	1.368 55	1.368 55	1.368 55
0.3	1.420 51	1.420 44	1.420 42	1.420 41	1.420 41	1.420 41	1.420 41
0.4	1.474 43	1.474 34	1.474 32	1.474 31	1.474 31	1.474 30	1.474 30
0.5	1.530 36	1.530 28	1.530 25	1.530 24	1.530 24	1.530 24	1.530 24
0.6	1.588 31	1.588 22	1.588 20	1.588 19	1.588 19	1.588 19	1.588 19
0.7	1.648 23	1.648 16	1.648 14	1.648 13	1.648 13	1.648 12	1.648 12
0.8	1.710 10	1.710 04	1.710 02	1.710 01	1.710 01	1.710 01	1.710 01
0.9	1.773 86	1.773 81	1.773 80	1.773 80	1.773 79	1.773 79	1.773 79
1.0	1.839 46	1.839 43	1.839 43	1.839 42	1.839 42	1.839 42	1.839 42

Table 3 Different orders of approximations of HAM solutions for β at $\hbar = -1$ with $M = 2$, $K = 1$

β	10th order	15th order	20th order	25th order	30th order	35th order	40th order
0.0	1.862 05	1.862 02	1.862 01	1.862 01	1.862 01	1.862 01	1.862 01
0.1	1.839 46	1.839 43	1.839 43	1.839 42	1.839 42	1.839 42	1.839 42
0.2	1.816 53	1.816 50	1.816 49	1.816 48	1.816 48	1.816 48	1.816 48
0.3	1.793 23	1.793 19	1.793 18	1.793 18	1.793 18	1.793 18	1.793 18
0.4	1.769 54	1.769 51	1.769 49	1.769 49	1.769 49	1.769 49	1.769 49
0.5	1.745 45	1.745 41	1.745 40	1.745 40	1.745 39	1.745 39	1.745 39
0.6	1.720 94	1.720 89	1.720 88	1.720 88	1.720 88	1.720 87	1.720 87
0.7	1.695 97	1.695 93	1.695 92	1.695 91	1.695 91	1.695 91	1.695 91
0.8	1.670 53	1.670 49	1.670 47	1.670 47	1.670 46	1.670 46	1.670 46
0.9	1.644 59	1.644 54	1.644 53	1.644 52	1.644 52	1.644 52	1.644 52
1.0	1.618 10	1.618 06	1.618 05	1.618 04	1.618 04	1.618 04	1.618 04

concluded that the results obtained are compatible with those in Ref. [4] by taking $\beta = 1$.

Figures 6 and 7 are prepared for f' against η for M, β and M, K, respectively. It is observed from Fig. 6 that when M increases, the velocity profile is more and more far away from the wall, and the boundary layer thickness is more and more thicker. Figure 7 indicates that when

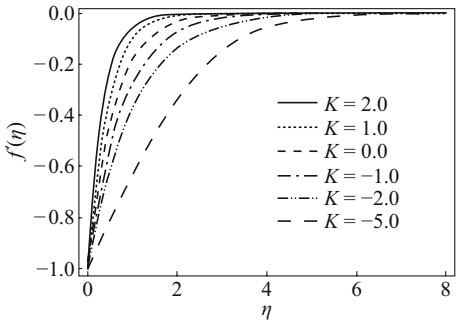

Fig. 4 Velocity profiles under different mass parameters K with $M = 4$ and $\beta = 1$

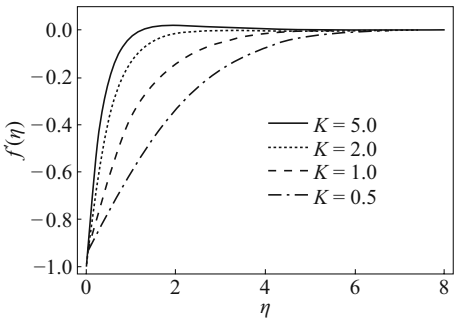

Fig. 5 Velocity profiles under different mass parameters K with $M = 1$ and $\beta = 1$

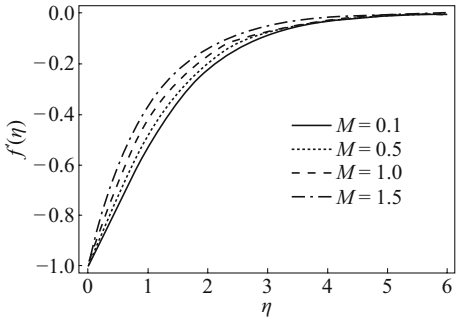

Fig. 6 Solution curves on f for different values of M with $K = 0.1$, $\beta = 0.1$

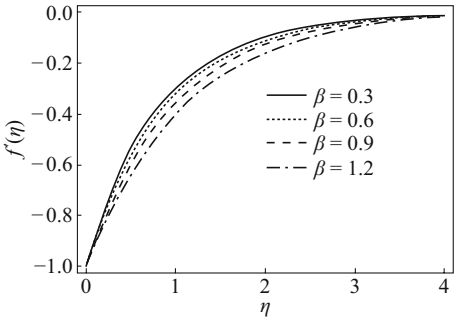

Fig. 7 Solution curves on f for different values of β with $M = 0.1$, $K = 0.1$

β increases, the velocity profile is more and more far away from the wall, whereas the boundary layer thickness increases.

4 Conclusions

In this paper, we have discussed the magnetohydrodynamic (MHD) flow of a viscous fluid towards a nonlinear porous shrinking sheet. The complete analytical solution of the boundary layer equation has been obtained by the homotopy analysis method (HAM). The solutions are compared with available results. They are compatible with each other. The convergence region showing the validity of the HAM solution is also computed. It is concluded that the HAM provides a simple and easy way to control and adjust the convergence region for strong nonlinearity and is applicable to highly nonlinear problems.

Acknowledgements The authors are thankful to the referees for their valuable suggestions.

References

[1] Fang, T., Liang, W., and Lee, C. F. A new solution branch for the Blasius equation—a shrinking sheet problem. *Comput. Math. Appl.* **56**(12), 3088–3095 (2008)

[2] Sajid, M. and Hayat, T. The application of homotopy analysis method for MHD viscous flow due to a shrinking sheet. *Chaos, Solitons & Fractals* **39**(3), 1317–1323 (2009)

[3] Hayat, T., Abbas, Z., Javed, T., and Sajid, M. Three-dimensional rotating flow induced by a shrinking sheet for suction. *Chaos, Solitons & Fractals* **39**(4), 1615–1626 (2009)

[4] Fang, T. and Zhang, J. Closed-form exact solutions of MHD viscous flow over a shrinking sheet. *Commun. Nonlinear Sci. Numer. Simulat.* **14**(7), 2853–2857 (2009)

[5] Fang, T. Boundary layer flow over a shrinking sheet with power-law velocity. *Int. J. Heat Mass Tran.* **51**(25-26), 5838–5843 (2008)

[6] Nadeem, S. and Awais, M. Thin film flow of an unsteady shrinking sheet through porous medium with variable viscosity. *Phys. Lett. A* **372**(30), 4965–4972 (2008)

[7] Hayat, T., Javed, T., and Sajid, M. Analytic solution for MHD rotating flow of a second grade fluid over a shrinking surface. *Phys. Lett. A* **372**(18), 3264–3273 (2008)

[8] Wang, C. Y. Stagnation flow towards a shrinking sheet. *Int. J. Non-Linear Mech.* **43**(5), 377–382 (2008)

[9] Hayat, T., Abbas, Z., and Ali, N. MHD flow and mass transfer of an upper-convected Maxwell fluid past a porous shrinking sheet with chemical reaction species. *Phys. Lett. A* **372**(26), 4698–4704 (2008)

[10] Chaim, T. C. Hydromagnetic flow over a surface stretching with a power law velocity. *Int. J. Eng. Sci.* **33**(3), 429–435 (1995)

[11] Abbas, Z., Wanga, Y., Hayat, T., and Oberlack, M. Hydromagnetic flow in a viscoelastic fluid due to the oscillatory stretching surface. *Int. J. Non-Linear Mech.* **43**(8), 783–793 (2008)

[12] Mohamed, R. A., Abbas, I. A., and Abo-Dahab, S. M. Finite element analysis of hydromagnetic flow and heat transfer of a heat generation fluid over a surface embedded in a non-Darcian porous medium in the presence of chemical reaction. *Commun. Nonlinear Sci. Numer. Simulat.* **14**(4), 1385–1395 (2009)

[13] Hayat, T. and Ali, N. A mathematical description of peristaltic hydromagnetic flow in a tube. *Appl. Math. Comput.* **188**(2), 1491–1502 (2007)

[14] Attia, H. A. Unsteady hydromagnetic Couette flow of dusty fluid with temperature dependent viscosity and thermal conductivity. *Int. J. Non-Linear Mech.* **43**(8), 707–715 (2008)

[15] Tsai, R., Huang, K. H., and Huang, J. S. The effects of variable viscosity and thermal conductivity on heat transfer for hydromagnetic flow over a continuous moving porous plate with Ohmic heating. *Appl. Therm. Eng.* **29**(10), 1921–1926 (2009)

[16] Ghosh, A. K. and Sana, P. On hydromagnetic flow of an Oldroyd-B fluid near a pulsating plate. *Acta Astronautica* **64**(2-3), 272–280 (2009)

[17] Chiam, T. C. Hydromagnetic flow over a surface stretching with a power-law velocity. *Int. J. Eng. Sci.* **33**(3), 429–435 (1995)

[18] Liao, S. J. Comparison between the homotopy analysis method and homotopy perturbation method. *Appl. Math. Comput.* **169**(2), 1186–1194 (2005)

[19] Abbasbandy, S. The application of homotopy analysis method to nonlinear equations arising in heat transfer. *Phys. Lett. A* **360**(1), 109–113 (2006)

[20] Liao, S. J. and Cheung, K. F. Homotopy analysis of nonlinear progressive waves in deep water. *J. Eng. Math.* **45**(2), 105–116 (2003)

[21] Liao, S. J. *Beyond Perturbation*: *Introduction to Homotopy Analysis Method*, Chapman and Hall/CRC Press, Boca Raton (2003)

[22] Rashidi, M. M., Domairry, G., and Dinarvand, S. Approximate solutions for the Burger and regularized long wave equations by means of the homotopy analysis method. *Commun. Nonlinear Sci. Numer. Simulat.* **14**(3), 708–717 (2009)

[23] Chowdhury, M. S. H., Hashim, I., and Abdulaziz, O. Comparison of homotopy analysis method and homotopy-perturbation method for purely non-linear fin-type problems. *Commun. Nonlinear Sci. Numer. Simulat.* **14**(2), 371–378 (2009)

[24] Bataineh, A. S., Noorani, M. S. M., and Hashim, I. On a new reliable modification of homotopy analysis method. *Commun. Nonlinear Sci. Numer. Simulat.* **14**(2), 409–423 (2009)

[25] Bataineh, A. S., Noorani, M. S. M., and Hashim, I. Modified homotopy analysis method for solving systems of second-order BVPs. *Commun. Nonlinear Sci. Numer. Simulat.* **14**(2), 430–442(2009)

[26] Bataineh, A. S., Noorani, M. S. M., and Hashim, I. Solving systems of ODEs by homotopy analysis method. *Commun. Nonlinear Sci. Numer. Simulat.* **13**(10), 2060–2070 (2008)

[27] Sajid, M., Ahmad, I., Hayat, T., and Ayub, M. Series solution for unsteady axisymmetric flow and heat transfer over a radially stretching sheet. *Commun. Nonlinear Sci. Numer. Simulat.* **13**(10), 2193–2202 (2008)

[28] Sajid, M. and Hayat, T. Comparison of HAM and HPM methods in nonlinear heat conduction and convection equations. *Nonlinear Analysis*: *Real World Applications* **9**(5), 2296–2301 (2008)

Appendix

$$f_m(\eta) = \sum_{n=0}^{2m+1} a_{m,n} \mathrm{e}^{-n\eta}.$$

$$f'_m(\eta) = \sum_{n=0}^{2m+1} (-n) a_{m,n} \mathrm{e}^{-n\eta} = \sum_{n=0}^{2m+1} a1_{m,n} \mathrm{e}^{-n\eta},$$

where $a1_{m,n} = (-n)a_{m,n}$.

$$f''_m(\eta) = \sum_{n=0}^{2m+1} (-n) a1_{m,n} \mathrm{e}^{-n\eta} = \sum_{n=0}^{2m+1} a2_{m,n} \mathrm{e}^{-n\eta},$$

where $a2_{m,n} = (-n)a1_{m,n}$.

$$f'''_m(\eta) = \sum_{n=0}^{2m+1} (-n) a2_{m,n} \mathrm{e}^{-n\eta} = \sum_{n=0}^{2m+1} a3_{m,n} \mathrm{e}^{-n\eta},$$

where $a3_{m,n} = (-n)a2_{m,n}$.

$$f'''_{m-1}(\eta) = \sum_{n=0}^{2m-1} a3_{m-1,n} \mathrm{e}^{-n\eta}.$$

$$f'_{m-1}(\eta) = \sum_{n=0}^{2m-1} a1_{m-1,n} \mathrm{e}^{-n\eta}.$$

$$\begin{aligned} f_{m-1-k} f''_k &= \sum_{r=0}^{2m-2k-1} a_{m-1-k,r} \mathrm{e}^{-r\eta} \sum_{s=0}^{2k+1} a2_{k,s} \mathrm{e}^{-s\eta} \\ &= \sum_{r=0}^{2m-2k-1} \mathrm{e}^{-(r+s)\eta} \sum_{s=0}^{2k+1} a2_{k,s} a_{m-1-k,r}. \end{aligned}$$

Let $r + s = n$.

$$f_{m-1-k} f''_k = \sum_{n=0}^{2m} \mathrm{e}^{-n\eta} \sum_{s=\max\{0,n-2m+2k+1\}}^{s=\min\{n,2k+1\}} a2_{k,s} a_{m-1-k,n-s}.$$

$$\begin{aligned} \sum_{k=0}^{m-1} f_{m-1-k} f''_k &= \sum_{n=0}^{2m} \mathrm{e}^{-n\eta} \left(\sum_{k=0}^{m-1} \sum_{s=\max\{0,n-2m+2k+1\}}^{s=\min\{n,2k+1\}} a2_{k,s} a_{m-1-k,n-s} \right) \\ &= \sum_{n=0}^{2m} \mathrm{e}^{-n\eta} \delta 1_{m,n}, \end{aligned}$$

where $\delta 1_{m,n} = \sum_{k=0}^{m-1} \sum_{s=\max\{0,n-2m+2k+1\}}^{s=\min\{n,2k+1\}} a2_{k,s} a_{m-1-k,n-s}$.

Similarly,

$$\sum_{k=0}^{m-1} f'_{m-1-k} f'_k = \sum_{n=0}^{2m} \mathrm{e}^{-n\eta} \delta 2_{m,n},$$

where

$$\delta 2_{m,n} = \sum_{k=0}^{m-1} \sum_{s=\max\{0,n-2m+2k+1\}}^{s=\min\{n,2k+1\}} a1_{k,s} a_{m-1-k,n-s}.$$

$$\begin{aligned}
\hbar \mathcal{R}_{1m}(\eta) &= f'''_{m-1}(\eta) - M^2 f'_{m-1}(\eta) + \sum_{k=0}^{m-1} \left(f_{m-1-k} f''_k - \beta f'_{m-1-k} f'_k \right), \\
&= \hbar \sum_{n=0}^{2m-1} \mathrm{e}^{-n\eta} \left(a3_{m-1,n} - M^2 a1_{m-1,n} \right) + \hbar \sum_{n=0}^{2m} \mathrm{e}^{-n\eta} \left(\delta 1_{m,n} - \beta \delta 2_{m,n} \right) \\
&= \hbar \sum_{n=0}^{2m+1} \chi_{2m-n+1} \mathrm{e}^{-n\eta} \left(a3_{m-1,n} - M^2 a1_{m-1,n} \right) \\
&\quad + \hbar \sum_{n=0}^{2m+1} \chi_{2m-n+1} \mathrm{e}^{-n\eta} \left(\delta 1_{m,n} - \beta \delta 2_{m,n} \right) \\
&= \sum_{n=0}^{2m+1} \nabla_{m,n} \mathrm{e}^{-n\eta},
\end{aligned}$$

where

$$\nabla_{m,n} = \hbar \chi_{2m-n+1} \left(a3_{m-1,n} - M^2 a1_{m-1,n} + \delta 1_{m,n} - \beta \delta 2_{m,n} \right).$$

$$\mathcal{L}[f_m(\eta) - \chi_m f_{m-1}(\eta)] = \hbar \mathcal{R}_{1m}(\eta) = \sum_{n=0}^{2m+1} \nabla_{m,n} \mathrm{e}^{-n\eta}.$$

Taking $\mathcal{L}^{-1}$ on both sides, we obtain

$$\begin{aligned}
f_m(\eta) - \chi_m f_{m-1}(\eta) &= \sum_{n=0}^{2m+1} \nabla_{m,n} \mathcal{L}^{-1} \mathrm{e}^{-n\eta} \\
&= \sum_{n=0}^{2m+1} \nabla_{m,n} \frac{\mathrm{e}^{-n\eta}}{D^3 + D^2} + c_1^m + c_2^m \eta + c_3^m \mathrm{e}^{-\eta} \\
&= \sum_{n=2}^{2m+1} \nabla_{m,n} \frac{\mathrm{e}^{-n\eta}}{-n^3 + n^2} + c_1^m + c_2^m \eta + c_3^m \mathrm{e}^{-\eta} \\
&= \sum_{n=2}^{2m+1} \nabla_{m,n} \frac{\mathrm{e}^{-n\eta}}{n^2 (1-n)} + c_1^m + c_2^m \eta + c_3^m \mathrm{e}^{-\eta} \\
&= -\sum_{n=0}^{2m+1} \nabla_{m,n+2} \frac{\mathrm{e}^{-(n+2)\eta}}{(n+2)^2 (n+1)} + c_1^m + c_2^m \eta + c_3^m \mathrm{e}^{-\eta}.
\end{aligned}$$

As $f_m(0) = 0$, $f'_m(0) = 0$, and $f'_m(\infty) = 0$,

$$0 = -\sum_{n=0}^{2m+1} \nabla_{m,n+2} \frac{1}{(n+2)^2 (n+1)} + c_1^m + c_3^m.$$

$$f'_m(\eta) - \chi_m f'_{m-1}(\eta) = -\sum_{n=0}^{2m+1} \nabla_{m,n+2} \frac{-(n+2)\mathrm{e}^{-(n+2)\eta}}{(n+2)^2 (n+1)} + c_2^m - c_3^m \mathrm{e}^{-\eta}.$$

As $f'_m(0) = 0$,

$$\begin{aligned}
0 &= \sum_{n=0}^{2m+1} \nabla_{m,n+2} \frac{n+2}{(n+2)^2 (n+1)} + c_2^m - c_3^m \\
&= \sum_{n=0}^{2m+1} \nabla_{m,n+2} \frac{1}{(n+2)(n+1)} + c_2^m - c_3^m.
\end{aligned}$$

As $f'_m(\infty) = 0$ and $0 = c_2^m$,

$$c_3^m = \sum_{n=0}^{2m+1} \nabla_{m,n+2} \frac{1}{(n+2)(n+1)}.$$

$$\begin{aligned} c_1^m &= \sum_{n=0}^{2m+1} \nabla_{m,n+2} \frac{1}{(n+2)^2(n+1)} - \sum_{n=0}^{2m+1} \nabla_{m,n+2} \frac{1}{(n+2)(n+1)} \\ &= \sum_{n=0}^{2m+1} \nabla_{m,n+2} \frac{1}{(n+1)(n+2)} \left(\frac{1}{n+2} - 1\right). \end{aligned}$$

$$\begin{aligned} f_m(\eta) = \chi_m f_{m-1}(\eta) &- \sum_{n=0}^{2m+1} \nabla_{m,n+2} \frac{\mathrm{e}^{-(n+2)\eta}}{(n+2)^2(n+1)} \\ &+ \sum_{n=0}^{2m+1} \nabla_{m,n+2} \frac{1}{(n+1)(n+2)} \left(\frac{1}{n+2} - 1\right) \\ &+ \sum_{n=0}^{2m+1} \nabla_{m,n+2} \frac{\mathrm{e}^{-\eta}}{(n+2)(n+1)}. \end{aligned}$$

$$\begin{aligned} \sum_{n=0}^{2m+1} a_{m,n} \mathrm{e}^{-n\eta} &= \chi_m \sum_{n=0}^{2m-1} a_{m-1,n} \mathrm{e}^{-n\eta} - \sum_{n=0}^{2m+1} \nabla_{m,n+2} \frac{\mathrm{e}^{-(n+2)\eta}}{(n+2)^2(n+1)} \\ &\quad + \sum_{n=0}^{2m+1} \nabla_{m,n+2} \frac{1}{(n+1)(n+2)} \left(\frac{1}{n+2} - 1\right) \\ &\quad + \sum_{n=0}^{2m+1} \nabla_{m,n+2} \frac{\mathrm{e}^{-\eta}}{(n+2)(n+1)} \\ &= \sum_{n=0}^{2m+1} \chi_m \chi_{2m-n+1} a_{m-1,n} \mathrm{e}^{-n\eta} - \sum_{n=0}^{2m+1} \nabla_{m,n+2} \frac{1}{(n+2)^2(n+1)} \mathrm{e}^{-(n+2)\eta} \\ &\quad + \sum_{n=0}^{2m+1} \nabla_{m,n+2} \frac{1}{(n+1)(n+2)} \left(\frac{1}{n+2} - 1\right) \\ &\quad + \sum_{n=0}^{2m+1} \nabla_{m,n+2} \frac{\mathrm{e}^{-\eta}}{(n+2)(n+1)}. \end{aligned}$$

$$a_{m,0} = \chi_m \chi_{2m+1} a_{m-1,0} + \sum_{n=0}^{2m+1} \nabla_{m,n+2} \frac{1}{(n+1)(n+2)} \left(\frac{1}{n+2} - 1\right).$$

$$a_{m,1} = \chi_m \chi_{2m} a_{m-1,1} + \sum_{n=0}^{2m+1} \nabla_{m,n+2} \frac{1}{(n+1)(n+2)}.$$

$$a_{m,n} = \chi_m \chi_{2m-n+1} a_{m-1,n} + \nabla_{m,n+2} \frac{\mathrm{e}^{-2\eta}}{(n+2)^2(n+1)}.$$